CrystEngComm

PAPER

Particle size effects in the kinetic trapping of a structurally-locked form of a flexible metal-organic framework

Received 00th January 20xx,
Accepted 00th January 20xx

DOI: 10.1039/x0xx00000x

www.rsc.org/

Oliver M. Linder-Patton[a], Witold M. Bloch[a,b], Campbell J. Coghlan[a], Kenji Sumida[a], Susumu Kitagawa[c], Shuhei Furukawa[c], Christian J. Doonan[a] and Christopher J. Sumby[a*]

The application of metal-organic frameworks (MOFs) for gas storage, molecular separations and catalysis neccesitates careful consideration of the particle size and structuralisation (e.g. pelletisation, surface-anchoring) of a material. Recently, particle size has been shown to dramatically alter the physical and structural properties of certain MOFs but overall there is limited information on how the particle size affects the properties of flexible MOFs. Here we demonstrate that the particle size of a flexible MOF, specifically the as-synthesised form of [Cu(**bcppm**)H_2O]·S (H_2**bcppm** = bis(4-(4-carboxyphenyl)-*1H*-pyrazolyl)methane, S = solvent) (**1**), correlates with the rate of structural reorganisation from a "kinetically-trapped" activated 3D form of this MOF to the "open" 2D form of the structure. We also outline two methods for synthetically reducing the particle size of **1** at room temperature, using 0.1 M NaOH (for two reaction times: 0.5 and 16 h) and with the sodium salt of the ligand Na_2**bcppm**, producing crystals of 85 ± 15, 280 ± 14 and 402 ± 41 nm, respectively.

Introduction

Metal-organic frameworks (MOFs) are versatile, highly porous materials whose pore size and functionality can be dictated by the organic ligands (linkers) and metal centres (nodes) that form the framework.[1-3] MOFs exhibiting structural flexibility represent a subset of these materials, and feature structural changes to their ordered coordination networks (crystal-to-crystal transformations), often reversibly and without changes in the bond sequences within the lattice.[4, 5] This includes transformations induced by host-guest interactions,[6, 7] and physical stimuli such as pressure,[8] light, and heat.[9-11] The properties associated with flexible MOFs have led to potentially diverse applications for these materials including molecular separations,[12] gas adsorption,[13-16] sensing,[17] drug delivery (guest capture and release)[18, 19] and catalysis.[5, 20, 21]

MOFs are conventionally synthesised under laboratory conditions that consistently produce micron size crystals, primarily due to ease of structural characterisation. While this is adequate for the discovery of new materials, the development of synthetic protocols[22-26] that also provide control over the crystal size (ideally in the nm range) and morphology is crucial if MOFs are to be tailored for specific applications.[27] Such methods are also expected to be crucial if MOFs are to be used in tandem with other materials, such as the solid phase additive within mixed matrix membranes (MMMs).[28, 29]

The particle size of MOFs has also been demonstrated to impart unique physical and structural properties to the materials when precisely controlled in the nanoscale regime.[30-33] Fundamentally, changes in the particle size will directly alter diffusion rates and surface-to-volume ratios, but more sophisticated changes have been observed.[30-33] One recent example reported that the crystal downsizing of a two-fold interpenetrated MOF exhibiting elastic flexibility (between an open and closed phase) resulted in the evolution of a third, metastable phase that affords a "shape memory" effect not seen in larger, micrometre-sized crystals.[32] In general, however, studies addressing the effect of particle size on the dynamic properties of MOFs (i.e. framework flexibility) remain rare, and more studies of this type are required prior to consideration of these materials for use in real-world applications. Herein, we specifically investigate the impact of particle size on a structural transformation that is controlled by inter-framework chemical bond formation.

We have previously reported a flexible copper(II) MOF, [Cu(**bcppm**)H_2O]·S (**1**·S, where H_2**bcppm** = bis(4-(4-carboxyphenyl)-*1H*-pyrazolyl)methane, S = solvent), which has exceptional CO_2/N_2 selectivity when activated.[34] This MOF

[a] *Department of Chemistry and Centre for Advanced Nanomaterials, School of Physical Sciences, The University of Adelaide, Adelaide, Australia. CJS: Fax: +61 8 8313 4358; Tel: +61 8 8313 7406; E-mail: christopher.sumby@adelaide.edu.au*
[b] *Present address: Department of Chemistry, Georg-August-University Göttingen, Göttingen, Germany.*
[c] *Institute for Integrated Cell-Material Sciences (WPI-iCeMS), Kyoto University, Kyoto, Japan.*

Electronic Supplementary Information (ESI) available: unit cell parameters, combined descriptions of the single crystal structures of [Cu(**bcppm**)H_2O]·S (S = as-synthesised, acetone, water, ethanol; heated sample), SEM images, Dynamic Light Scattering data, PXRD data, UV-vis transmittance data, gas adsorption data and additional synthetic data. See DOI: 10.1039/x0xx00000x

undergoes an intriguing structural transformation from a flexible 2D layered material to a "locked" 3D framework upon activation.[34] The role of this structural "locking" is of significant importance to the properties of the framework, and herein we show that this is a reversible particle size-dependent process. We report two methods of synthesising **1**·S at room temperature (RT) which afford a dramatic reduction in particle size. The first utilises a strong base to promote rapid deprotonation of the dicarboxylic acid H_2**bcppm**, inspired by the pH control achieved by Zhang *et al*.[35] The second uses the sodium salt of the ligand, Na_2**bcppm**, in MOF synthesis, drawing from work recently published by Díaz *et al*.[36] We report structural flexibility of the as-synthesised 2D form of the framework and show that particle size correlates with the rate of structural reorganisation of **1** - a 'kinetically trapped' form - to the 'open' material, **1**·S.

Experimental

General considerations

All materials were purchased commercially unless otherwise stated. The ligand bis(4-(4-carboxyphenyl)-*1H*-pyrazolyl)methane (H_2**bcppm**) was prepared according to literature methods.[34] Micron-scale crystals of [Cu(**bcppm**)H_2O]·S (**1**·S; S = solvate) and the activated form, [Cu(**bcppm**)H_2O] (**1**) were also prepared by the procedure of Bloch *et al*.[34] The solvated samples reported were obtained by soaking samples of **1**·S in millilitre volumes of various solvents (acetone, ethanol or water) overnight, or in the case of the heated material by heating a sample of **1**·ethanol on a microscope slide at 85°C for 1 h. Details of the single crystal X-ray structure determinations of the solvent-exchanged forms of **1** are given in the supporting information (Table S1).

Samples for dynamic light scattering (DLS) experiments using a Malvern Zetasizer Nano series (λ = 671 nm) were prepared by suspending each material in excess methanol. A few drops (less than 5) of each solution were added to a cuvette containing methanol (1 ml), and this solution was mixed and sonicated for 5 minutes prior to the DLS experiment.

Scanning electron microscopy (SEM) images were collected on a Philips XL30 scanning electron microscope at Adelaide Microscopy. Samples were dry-loaded onto adhesive carbon tabs on aluminium stubs and coated with carbon.

Solid-state UV/vis transmittance spectroscopy was recorded on a Varian Cary 5000 UV/vis spectrometer with Harrick Praying Mantis DRP accessory. Dried samples were loaded (< 10 mg) and packed flat on the plate. %T spectra were collected between 300 and 800 nm. Infrared spectra were collected on a Perkin-Elmer Spectrum 100 using a universal attenuated total reflectance (UATR) sampling accessory.

Gas adsorption isotherm measurements were performed on an ASAP 2020 Physisorption Analyser. UHP grade (99.999%) N_2 and CO_2 were used for all measurements. The temperatures were maintained at 77 K (liquid nitrogen bath) and 293 K (room temperature water bath).

Powder X-ray diffraction data was collected on a Bruker D8-Advanced X-ray powder diffractometer (parallel X-ray, capillary loaded) using a Cu Kα (λ =1.5418 Å) radiation source. Samples were mounted in 0.5 mm glass capillaries and data collected for between 2θ of 2° to 52.94° with Phi rotation at 20 rotations/min at 1 second exposure per step at 5001 steps. The data were then converted into xye format and background subtracted using WinPlotr 2000 software.[37] Simulated powder X-ray diffraction patterns were generated from the single crystal X-ray data using Mercury 3.5.1.[38, 39]

Synthesis of materials

Synthesis of Na_2bcppm. H_2**bcppm** (0.5 g, 1.28 mmol) and NaOH (1.3 ml, 2 M) were stirred until the solution became clear. The solvent was removed under reduced pressure to give a white solid Na_2**bcppm** (0.532 g, 96%). M.P.: >260°C. ^{1}H NMR (500 MHz/DMSO): δ 6.40 (s, 2H, CH_2), 7.46 (d, 4H, H2'/H6'), 7.80 (d, 4H, H3'/H5'), 7.95 (s, 2H, H3 or H5), 8.39 (s, 2H, H3 or H5). ^{13}C NMR (500 MHz/DMSO): δ 66.0, 121.0, 125.0, 128.0, 128.7, 130.0, 136.5, 138.7, 170.0.

General room temperature synthesis of [Cu(bcppm)H_2O]·S (S = solvate) using the base NaOH (1b·S where b = base). In a 20 ml screw cap vial, $Cu(NO_3)_2$·2.5H_2O (36.0 mg, 0.16 mmol) and H_2**bcppm** (41.5 mg, 0.11 mmol) were dissolved in a mixture of DMF (2 ml) and ethanol (0.5 ml). Sodium hydroxide 0.1 M (0.5 ml) was injected into the stirred solution. The resultant solution was stirred for a period of time (0.5 - 16 hours) at room temperature. The product was washed with DMF (×2) and methanol (×5) to give a light blue microcrystalline material (8 mg, 16%)

General room temperature synthesis of [Cu(bcppm)H_2O]·S (S=solvate) using the ligand salt Na_2bcppm (1s·S, where s = salt). In a 20 ml screw cap vial, $Cu(NO_3)_2$·2.5H_2O (36.0 mg, 0.16 mmol) dissolved in DMF (2 ml) and in a separate vial Na_2**bcppm** (44.1 mg, 0.11 mmol) was dissolved in a mixture of ethanol (0.5 ml), water (0.5 ml). The ligand solution was injected into the stirred copper(II) solution and the resultant solution was stirred for a period of time (0.5 - 16 hours). The product was washed with DMF (×2) and methanol (×5) resulting in a light blue microcrystalline material (23 mg, 46%)

Activation procedure. The as-synthesised samples were washed with DMF (×2) and acetone (×7), dried under a nitrogen flow, and then heated under a high vacuum at 120 °C for 1 hour. Activation yielded light green microcrystalline powders for both samples **1b** and **1s**.

Results and discussion

Structural flexibility of 1

Single-crystals of [Cu(**bcppm**)H_2O]·S (**1**·S) prepared by the conventional solvothermal method[34] were initially used for a series of single-crystal X-ray structure determinations. The structural flexibility of the as-synthesised 2D form **1** was probed by a series of single crystal X-ray structure

determinations on solvent exchanged forms and also for a heated sample, which affords a structure consistent with the 'locked' 3D phase obtained following activation (Fig. 1). All structure determinations confirmed the formulation of the MOF as reported previously for [Cu(**bcppm**)H_2O]·S[34] but with the changes in the unit cell parameters, described below, that represent the breathing of the MOF. For completeness, structure descriptions are provided in the supporting information but only the unit cell changes are discussed here. In all cases, the samples underwent structural changes in a single-crystal to single-crystal process. The solid-state structure of **1**·acetone revealed a subtle increase in the *a* axis (along the pore channel direction), an increase in the *b* axis, and a decrease in the *c* axis, relative to as-synthesised **1**·S (containing predominantly DMF in the voids, Fig. 1a).[34] Similar changes to the *b* and *c* axis were observed for the water- and ethanol-exchanged samples, although in these cases, a reduction of the *a* axis was observed, (Fig. 1a and Table S2). This small *a*-axis contraction for **1**·ethanol and **1**·water corresponds to a reduction of the interlayer separation and is indicative of closer contact between the water ligands bound to the Cu centres of one layer and the Cu atoms in an adjacent 2D layer, en-route to the formation of the bridging water ligand as identified in the 3D 'locked' form.[34] The most dramatic changes in these samples occurred in the *b* and *c* axes, resembling a trellis-type rearrangement (Fig. 1b and 1c) and an overall structural contraction as indicated by the cell volume. This indicates that the MOF is indeed flexible and responds structurally to guest exchange along all three axes.

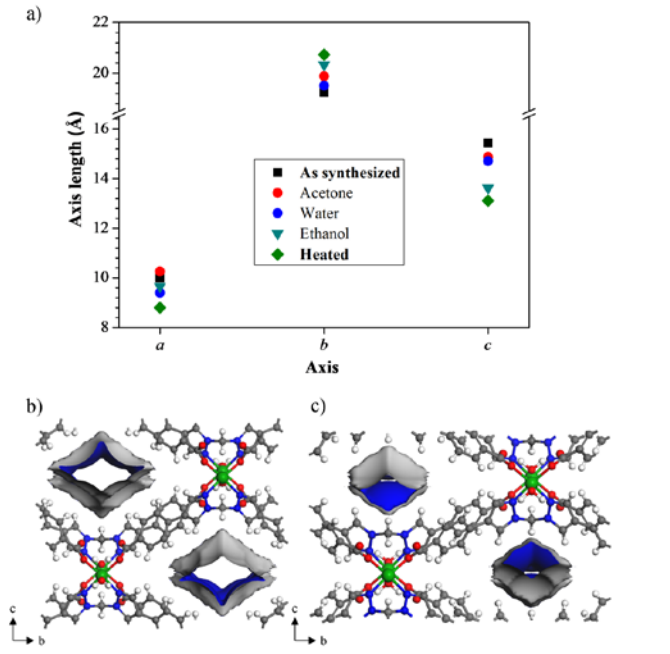

Fig. 1. a) A plot of the crystallographic cell parameters of solvent exchanged samples of **1**. b) A portion of the crystal structure of as-synthesised **1**·S and c) after heating and partial desolvation at 80 °C. Green, gray, blue, red, and white spheres represent Cu, C, N, O, and H atoms, respectively. The contours in the diagram represent the solvent-accessible pore surface as probed with a 3.3 Å sphere.

As we reported previously,[34] an even more dramatic change was observed when **1**·EtOH was heated at 85°C for 1 hour (slightly lower than used to obtain the activated form), yielding a partially desolvated sample. This form has a significantly reduced cell volume, due to a prominent trellis-like contraction of the *c*-axis and elongation of the *b*-axis. In contrast to the solvent exchanged forms, a considerable contraction of the *a*-axis was observed in this partially desolvated sample corresponding to a change in the coordination environment of the copper(II) centre from five coordinate to a Jahn-Teller distorted octahedral six coordinate. The water ligand bridges the 2-D layers (Cu1-O1 = 2.265Å, O1-Cu1a = 2.397 Å, symmetry code: $^1/_2+x$, $^1/_2-y$, $^3/_2z$) to form the 'locked' 3D structure.

Particle size control of 1

Having established the structural flexibility of **1**, we investigated methods to systematically vary the particle size. Solvothermal synthesis of **1** by the literature procedure,[34] produced large, dark-blue block-shaped crystals approximately 50–100 μm in size (Fig. 2d). Since the formation of the framework must necessarily proceed via deprotonation of the carboxylate groups, we surmised that increasing the pH of the reaction mixture would promote rapid deprotonation of carboxylate ligands, facilitating faster nucleation and a greater number of nucleation sites to give smaller crystals.[30, 35] Indeed, the use of basic conditions (0.1 M NaOH) over 16 h at room temperature afforded uniform crystals of **1b**·S (where b = base) approximately 200–300 nm in size (Fig. 2b). Under similar conditions, using the sodium salt of the dicarboxylic acid, Na_2**bcppm**, produced crystals of **1s**·S (where s = salt) approximately 500 nm in size (Fig. 2c, see also Fig. S3). Powder X-ray diffraction (Fig. S6) confirmed that both **1b**·S and **1s**·S were phase-pure, while dynamic light scattering (DLS) experiments revealed that the basic conditions produced a narrower distribution of crystal sizes than the ligand salt conditions, with average sizes of 280 ± 14 nm and 402 ± 41 nm, respectively (Fig. S4).

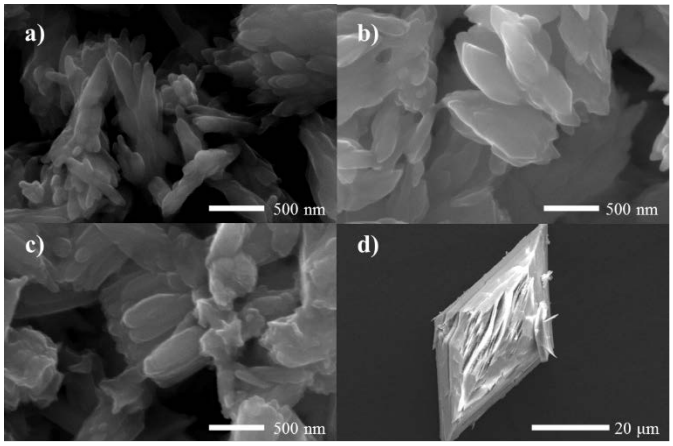

Fig. 2. SEM images of crystals of **1** prepared at room temperature using a reaction solution containing 0.1 M NaOH over a) 0.5 h and b) 16 h, or c) with Na_2**bcppm** over 16 h, and d) a conventional preparation over 16 h.

Experiments conducted using variable reaction times demonstrated that nucleation occurs rapidly (< 0.5 h), as shown by a DLS measurement conducted after 30 minutes (85 ± 15 nm, see Fig. 2a, Fig. S5). Beyond the initial nucleation events (> 0.5 h), there is a period of continuing crystal growth, shown by the broad distributions of particle size at 1.0 and 1.5 h, before particle size plateaus from 1.5 h, likely resulting from limited remaining (deprotonated) ligand in solution. In relation to these observations there are two potential mechanisms of crystal growth at room temperature which have been described in the literature, (a) fast initial nucleation followed by slow crystal growth and (b) slow nucleation followed by rapid crystal growth.[35, 40] Mechanism (a) results in a narrow distribution of particle sizes, whereas (b) results in a broad distribution of particle sizes.[35, 40, 41] However, these studies utilised capping agents, such as sodium acetate, to modulate crystal growth after initial deprotonation.[25] The time course experiments conducted here did not utilise a capping agent and so the growth rate was not modulated. As such, a broader distribution of crystal size was observed during the growth phase, consistent with rapid uninhibited crystal growth.

The reactant concentration and ligand-to-base ratio were also systematically varied to establish their effect on the particle size of **1** (Fig. 3). Here, three levels were selected for the concentration (12 mM, 18 mM and 36 mM in the H_2**bcppm** ligand) and the ligand-to-base ratio (2:1, 1:1 and 1:2), giving a total of nine samples for analysis. Isolation of the solids that emerged in each reaction after 0.5 h followed by particle size analysis using DLS revealed two main trends (see Fig. 3). Firstly, the particle size increased when the amount of base was increased (ligand-to-base ratio from 2:1 to 1:2). Secondly, particle size increased when the reactant concentration was reduced. The nine entries in Fig. 3 were each verified to be **1** by PXRD (Fig. S7 and Table S3). These experiments revealed that reducing the concentration of reactants, from 36 mM of ligand (the limiting reagent) to 12 mM, promoted the growth of larger crystals, as seen in all three ligand-to-base ratios (Fig. 3). This observation is consistent with a decrease in the reactant concentration causing the nucleation of crystals to be more limited, hence allowing the growth of larger crystals. This is in contrast to the coordination modulation approach[41] that gives larger crystals when increasing the concentration, although it must be noted that the concentration was decreased by adding solvent rather than using less reagent (convection and other mass transport phenomena may thus also play a role).

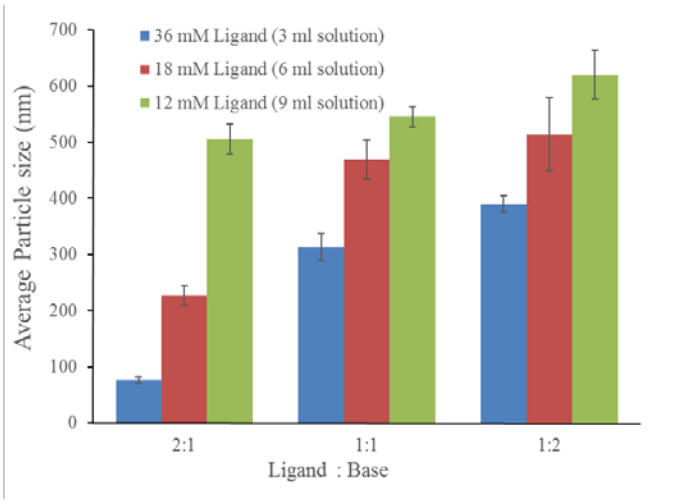

Fig. 3. Average particle size of **1b**·S after 0.5 h by altering the concentration of H_2**bcppm** and the ligand to base ratio from 2:1 to 1:1 and 1:2.

Increasing the amount of base appears to have two effects: expediting the rate of nucleation but also accelerating crystal growth. Raising the pH of a reaction mixture has previously been shown to facilitate deprotonation of carboxylate ligands which in turn leads to an increase in nucleation rate.[30, 35] In the context of this work, the ligand-base ratios; 2:1, 1:1 and 1:2 correspond to a mole ratio of carboxylic acid groups to base in solution of 4:1, 2:1 and 1:1 respectively as H_2**bcppm** is a dicarboxylic acid. Thus increasing the amount of NaOH added to the solution engenders a greater concentration of deprotonated ligand in solution and presumably accelerates nucleation. However, while a reduction in crystal size was expected under these conditions, crystal growth has been accelerated as a consequence of having more ligand available in solution and no competition from a suitable modulator. Thus, it appears that the change of parameters predominantly influences the growth process. We suggest that the increase in pH provides more ligand for a limited number of nuclei to grow larger, while the reduction in overall concentration will decrease the number of nuclei formed in the nucleation process and thus gives larger crystals due to the rapid, non-modulated growth process.

Overall, greater control of particle size has been achieved at room temperature with addition of NaOH, affording crystals from 85 nm to 620 nm, by judiciously modifying the reactant concentration and ligand-to-base ratio. All materials obtained by these varied synthetic methods retain the structural flexibility that is a hallmark of the as-synthesised material.

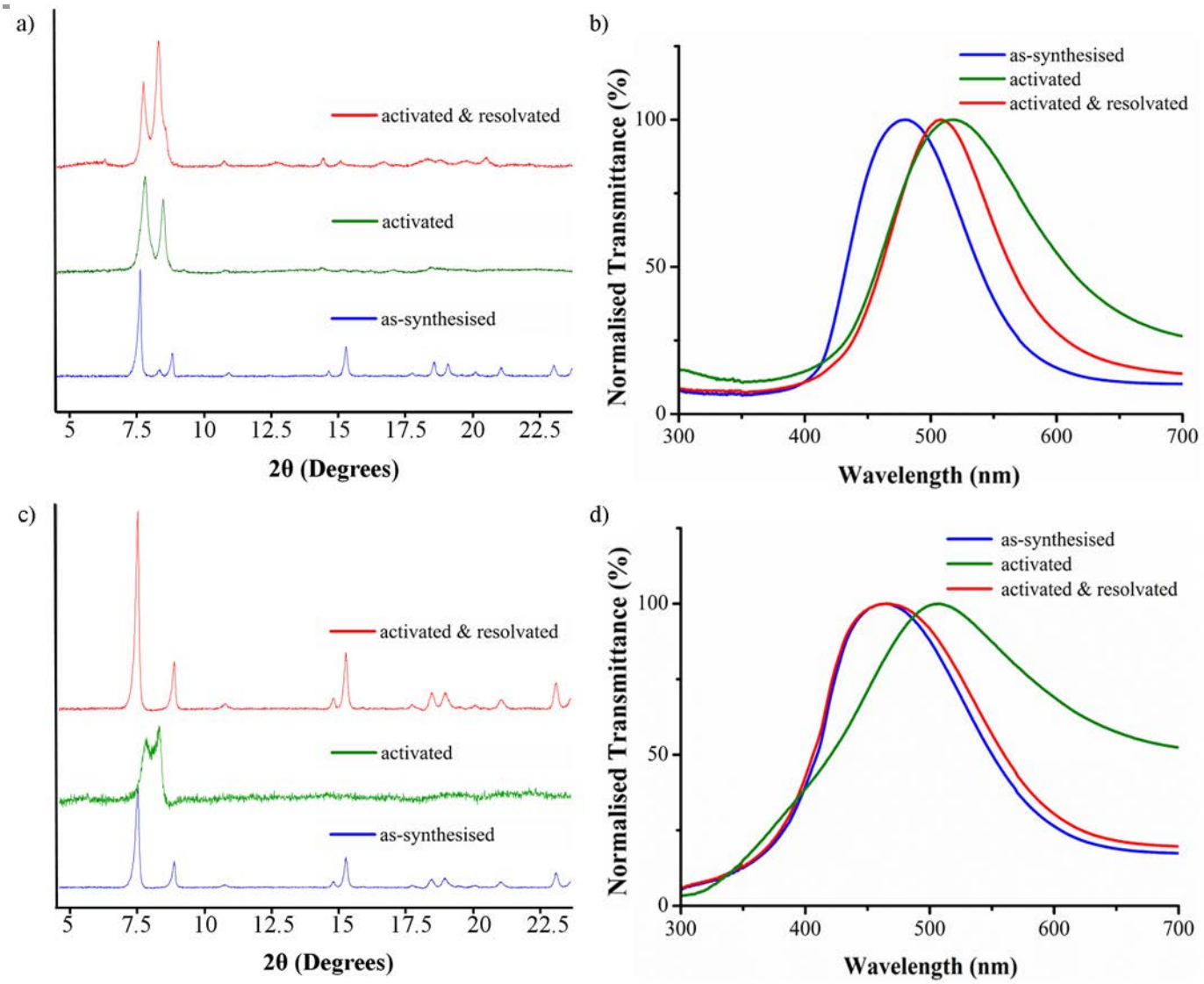

Fig. 5. a) Powder X-ray diffraction patterns and b) solid-state UV/vis transmittance spectra of a methanol-exchanged sample of **1**·S (blue), **1** (green) and **1**·MeOH obtained by resolvation of an activated sample of **1** in methanol overnight (red), c) Powder X-ray diffraction patterns and d) solid state UV/vis transmittance spectra of a methanol-exchanged sample of **1s**·S (blue), **1s** (green) and **1**·MeOH obtained by resolvation of an activated sample of **1s** in methanol overnight (red). In the PXRD plots the peaks at *ca.* 2θ = 7.5° and 2θ = 8.5° correspond to 011 and 020 planes respectively which reflect the breathing of the MOF. In the sample of **1**·S (blue) the peak at *ca.* 2θ = 8.0° corresponds to a small amount of the dried sample which forms as the material is packed into the capillaries.

Kinetic trapping of the 3D locked form of 1

MOF **1** can be post-synthetically modified by heating a solvent-exchanged sample at 120°C, thus removing pore bound solvent and activating the material to produce the activated form of **1**. As previously reported, during this process the 2D trellis-like framework 'locks' into a permanently porous 3D framework (Fig. 4),[34] and the coordination environment of the copper(II) centre changes from five coordinate square pyramidal to a six coordinate octahedral Jahn-Teller distorted geometry. The apparent 'locking' of the framework occurs when the coordinated water ligand on one copper centre coordinates to the vacant site on the square plane of the adjacent centre.[34]

During activation there is a distinct colour change, from blue to green, that results from a change in coordination environment.[34] This distinctive colour change was examined by solid-state UV/vis transmittance spectroscopy, with the maxima shifting from 480 nm (blue) to 500 nm (green), (Fig. 5b). Additionally, the structural change can be observed in the PXRD pattern (Fig. 5a), in which there is a distinct shift in the spacing of 011 (*ca.* 2θ = 7.5°) and 020 (*ca.* 2θ = 8.5°) planes. PXRD and UV-vis transmittance spectroscopy both confirm that 50-100 μm sized crystals of **1** could not be 'unlocked' by re-solvation in methanol, even when heated at 65°C.[34] By carefully monitoring samples of **1** exposed to methanol it was noted that the 50-100 μm 'bulk' crystals took 7 days to

undergo a transformation back into the as-synthesised structure (Fig. S8).

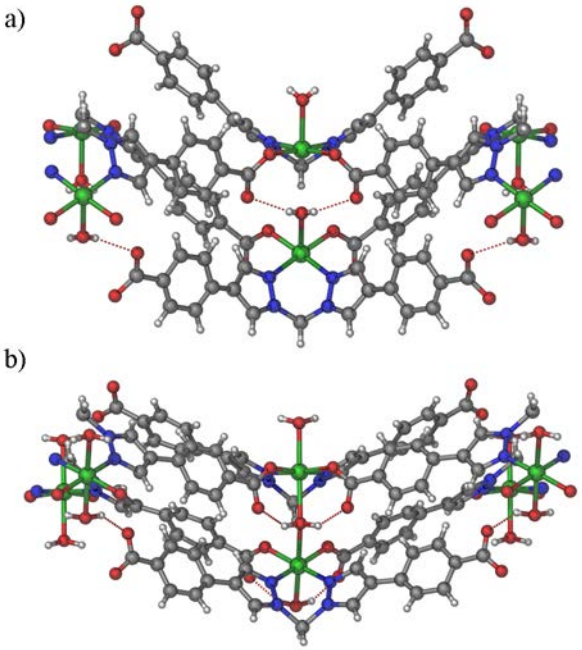

Fig. 4. The coordination environment of copper(II) centres in a) **1**·S and b) **1,** where the dotted red lines denote hydrogen bonding.[34] Green, grey, blue, red and white spheres represent Cu, C, N, O, and H atoms, respectively.

Compared to solvothermally synthesised **1**, decreasing the particle size to 280 ± 14 and 402 ± 41 nm (samples **1b** and **1s** respectively) increases the rate of structural reorganisation. Upon resolvation overnight in methanol, PXRD confirm that both **1s**·MeOH and **1b**·MeOH rapidly attain the as-synthesised 'open' structure, (Fig. 5c and S9). In the transmittance spectra there is a notable maxima shift for the resolvated material, from 500 nm to 480 nm (Fig. 5d and S9), indicating a change in coordination environment from six to five coordinate, consistent with the as-synthesised form. The rate of structural reorganisation for sub-micron samples was investigated via a series of PXRD experiments. Samples of **1b** (at 0.5 and 16 h) and **1s** (at 16 h), were investigated by collecting PXRD patterns every 90 minutes following immersion in methanol. The submicron samples of **1** demonstrate rapid structural reorganisation and 'unlocking' within 3 h of resolvation in methanol (Fig. 6, S10 and S11), which is significantly faster than observed in micron-sized crystals.

Crystal size and the synthesis conditions are the two factors that differ between the bulk and submicron samples. To eliminate potential influence of the synthetic conditions on the rate of "unlocking" of **1**, a sample of **1** was synthesised using conventional solvothermal conditions (giving large crystals approximately 50-100 µm in size) followed by mechanical grinding to give a sample with a broad range of crystallite sizes from 1 to 10 µm, (Fig. S12). Despite the broad particle size distribution, the as-synthesised structure was reformed upon resolvation in methanol overnight (Fig. S12). This indicates that the rate of structural unlocking for **1** is not an artefact of the synthetic conditions, but rather originates from a decrease in the particle size.

The diffusion of solvent through the crystal structure is the likely factor mediating structural rearrangement. The kinetic diameter of methanol is 3.6 Å, which is slightly larger than the pore size of **1** (3.58 Å), and diffusion through the pores is likely to be slow at room temperature.[34, 42] Submicron sized crystals (280 and 402 nm) of **1** have the same pore size distribution as determined from a fitting to the CO_2 isotherms collected at 273 K (Fig. S13).[34, 43] Therefore, diffusion of methanol through all samples should occur at the same rate. However, decreasing the average crystal size is expected to reduce the time required for solvation of the crystal and full structural conversion of **1**.

Gas adsorption studies were conducted to assess the porosity of **1**, **1b** and **1s**. **1** is non porous to N_2 at 77 K, but due to increased external surface area, from decreasing crystal size, the sub-micron crystals of **1b** and **1s** yielded isotherms that are best described as type II (Fig. S14).[44] In addition, a decrease in overall uptake of CO_2 and a small increase in N_2 uptake at 293 K for **1b** and **1s** afforded a decreased N_2/CO_2 selectivity compared to that previously reported for their micron-sized counterparts[30] (Fig. S15 and Table S4).

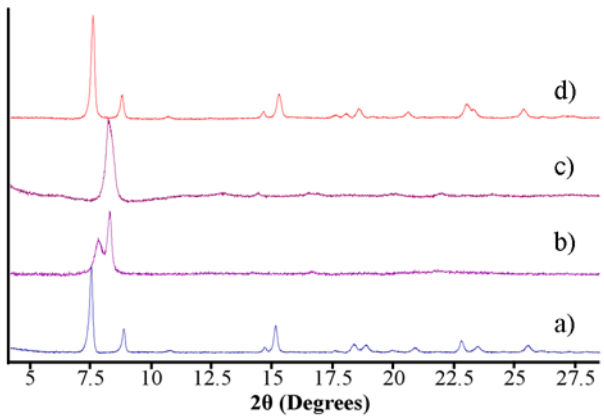

Fig. 6. PXRD of (a) **1b**·S (at 0.5 h), (b) **1b**, and **1b** after immersion in methanol for (c) 1.5 h and (d) 3 h.

Conclusions

The foregoing work has described two synthetic strategies for controlled crystal size reduction of the flexible MOF Cu(**bcppm**)H_2O (**1**): a room temperature synthesis with 0.1 M NaOH (**1b**, 0.5 and 16 h), and a synthesis using the salt of the linker, Na_2**bcppm** (**1s**). These strategies both produced sub-micron crystals of 85 ± 15, 280 ± 14 (**1b** after 0.5 and 16 h), and 402 ± 41 nm for **1s**, respectively. Examining the reaction time revealed a possible mechanism of nucleation under strong basic conditions involving rapid nucleation and unmediated crystal growth from conditions rich in deprotonated ligand. Particle size was further controlled at room temperature with NaOH by varying the reactant concentration and base-to-ligand ratio, affording crystals of different sizes in the range from 85 to 620 nm.

We have shown that the crystal size of **1** correlates with the rate of structural reversibility from the "kinetically-trapped form" to the "open form" of the material. Decreasing the crystal size of **1** reduces the timescale of the "unlocking" step from 7 days for the 'bulk' material to within 3 h for sub-micron samples. The increased rate of structural reorganisation presumably originates from more rapid solvent diffusion into the smaller crystals relative to 'bulk' crystals, due to a larger external surface area of the submicron samples and the shorter distance required for methanol to percolate in the smaller crystals. Thus, particle size has been demonstrated to dramatically alter the physical properties of **1** with regard to structural reorganisation. These observations demonstrate that due consideration must be given before applying MOFs, particularly those with flexible structures, to applications without first examining the properties of the material in the morphology to be utilised.

Acknowledgements

This research is supported by the Science and Industry Endowment Fund (SIEF). CJD and CJS would like to acknowledge the Australian Research Council for funding FT100100400 and FT0991910, respectively. CJS also acknowledges a Japan Society for the Promotion of Science for an International Incoming Fellowship (Long-term). KS thanks the Australian Research Council for funding DE160100306. iCeMS is supported by World Premier International Research Initiative (WPI), MEXT, Japan.

References

1 (a) H. Furukawa, K. E. Cordova, M. O'Keeffe and O. M. Yaghi, *Science*, 2013, **341**, 974; (b) M. Li, D. Li, M. O'Keeffe and O. M. Yaghi, *Chem. Rev.*, 2014, **114**, 1343–1370.

2 (a) O. M. Yaghi, M. O'Keeffe, N. W. Ockwing, H. K. Chae, M. Eddaoudi and J. Kim, *Nature*, 2003, **423**, 705; (b) S. Kitagawa, R. Kitaura and S. Noro, *Angew. Chem., Int. Ed.*, 2004, **43**, 2334; (c) G. Férey, *Chem. Soc. Rev.*, 2008, *37*, 191.

3 For recent reviews covering the emerging applications of metal-organic frameworks, refer to the special themed issues in *Chem. Rev.*, and more recently *Chem. Soc. Rev.*: (a) H.-C. Zhou, J. R. Long and O. M. Yaghi, *Chem. Rev.* 2012, **112**, 673; (b) H.-C. Zhou and S. Kitagawa, *Chem. Soc. Rev.* 2014, **43**, 5415, and references therein.

4 S. Horike, S. Shimomura and S. Kitagawa, *Nat. Chem.*, 2009, **1**, 695-704.

5 A. Schneemann, V. Bon, I. Schwedler, I. Senkovska, S. Kaskel and R. A. Fischer, *Chem. Soc. Rev.*, 2014, **43**, 6062-6096.

6 P. K. Thallapally, J. Tian, M. R. Kishan, C. A. Fernandez, S. J. Dalgarno, P. B. McGrail, J. E. Warren and J. L. Atwood, *J. Am. Chem. Soc.*, 2008, **130**, 16842-16843.

7 S. Henke, A. Schneemann, A. Wutscher and R. A. Fischer, *J. Am. Chem. Soc.*, 2012, **134**, 9464-9474.

8 S. A. Moggach, T. D. Bennett and A. K. Cheetham, *Angew. Chem. Int. Ed. Engl.*, 2009, **48**, 7087-7089.

9 S. Henke, A. Schneemann and R. A. Fischer, *Adv. Funct. Mater.*, 2013, **23**, 5990-5996.

10 A. Modrow, D. Zargarani, R. Herges and N. Stock, *Dalton transactions*, 2011, **40**, 4217-4222.

11 Y. Liu, J.-H. Her, A. Dailly, A. J. Ramirez-Cuesta, D. A. Neumann and C. M. Brown, *J. Am. Chem. Soc.*, 2008, **130**, 11813-11818.

12 J. R. Li, J. Sculley and H. C. Zhou, *Chem. Rev.*, 2012, **112**, 869-932.

13 A. Demessence, D. M. D'Alessandro, M. L. Foo and J. R. Long, *J. Am. Chem. Soc.*, 2009, **131**, 8784-8786.

14 J. Liu, P. K. Thallapally, B. P. McGrail, D. R. Brown and J. Liu, *Chem. Soc. Rev.*, 2012, **41**, 2308-2322.

15 K. Sumida, D. L. Rogow, J. A. Mason, T. M. McDonald, E. D. Bloch, Z. R. Herm, T. H. Bae and J. R. Long, *Chem. Rev.*, 2012, **112**, 724-781.

16 B. Seoane, J. Coronas, I. Gascon, M. Etxeberria Benavides, O. Karvan, J. Caro, F. Kapteijn and J. Gascon, *Chem. Soc. Rev.*, 2015, **44**, 2421-2454.

17 Z. Chang, D. H. Yang, J. Xu, T. L. Hu and X. H. Bu, *Adv. Mater.*, 2015, **27**, 5432-5441.

18 D. Cunha, M. Ben Yahia, S. Hall, S. R. Miller, H. Chevreau, E. Elkaïm, G. Maurin, P. Horcajada and C. Serre, *Chem. Mater.*, 2013, **25**, 2767-2776.

19 A. C. McKinlay, J. F. Eubank, S. Wuttke, B. Xiao, P. S. Wheatley, P. Bazin, J. C. Lavalley, M. Daturi, A. Vimont, G. De Weireld, P. Horcajada, C. Serre and R. E. Morris, *Chem. Mater.*, 2013, **25**, 1592-1599.

20 K. Uemura, R. Matsuda and S. Kitagawa, *J. Solid State Chem.*, 2005, **178**, 2420-2429.

21 S. Li and F. Huo, *Nanoscale*, 2015, **7**, 7482-7501.

22 M. Gimeno-Fabra, A. S. Munn, L. A. Stevens, T. C. Drage, D. M. Grant, R. J. Kashtiban, J. Sloan, E. Lester and R. I. Walton, *Chem Commun.*, 2012, **48**, 10642-10644.

23 J. Klinowski, F. A. Paz, P. Silva and J. Rocha, *Dalton*, 2011, **40**, 321-330.

24 A. Pichon, A. Lazuen-Garay and S. L. James, *CrystEngComm*, 2006, **8**, 211.

25 T. Friscic, *Chem. Soc. Rev.*, 2012, **41**, 3493-3510.

26 S. L. James, C. J. Adams, C. Bolm, D. Braga, P. Collier, T. Friscic, F. Grepioni, K. D. Harris, G. Hyett, W. Jones, A. Krebs, J. Mack, L. Maini, A. G. Orpen, I. P. Parkin, W. C. Shearouse, J. W. Steed and D. C. Waddell, *Chem. Soc. Rev.*, 2012, **41**, 413-447.

27 N. Stock and S. Biswas, *Chem. Rev.*, 2012, **112**, 933-969.

28 A. Betard and R. A. Fischer, *Chem. Rev.*, 2012, **112**, 1055-1083.

29 H. B. Tanh Jeazet, C. Staudt and C. Janiak, *Dalton*, 2012, **41**, 14003-14027.

30 C. Zhang, J. A. Gee, D. S. Sholl and R. P. Lively, *J. Phys. Chem. C*, 2014, **118**, 20727-20733.

31 H. Uehara, S. Diring, S. Furukawa, Z. Kalay, M. Tsotsalas, M. Nakahama, K. Hirai, M. Kondo, O. Sakata and S. Kitagawa, *J. Am. Chem. Soc.*, 2011, **133**, 11932-11935.

32 Y. Sakata, S. Furukawa, M. Kondo, K. Hirai, N. Horike, Y. Takashima, H. Uehara, N. Louvain, M. Meilikho, T. Tsuruoka, S. Isoda, W. Kosaka, O. Sakata and S. Kitagawa, *Science*, 2013, **339**, 193-196.

33 J. Zhou, X. Yu, X. Fan, X. Wang, H. Li, Y. Zhang, W. Li, J. Zheng, B. Wang and X. Li, *J. Mater. Chem. A*, 2015, **3**, 8272-8275.

34 W. M. Bloch, R. Babarao, M. R. Hill, C. J. Doonan and C. J. Sumby, *J. Am. Chem. Soc.*, 2013, **135**, 10441-10448.

35 H. Guo, Y. Zhu, S. Wang, S. Su, L. Zhou and H. Zhang, *Chem. Mater.*, 2012, **24**, 444-450.

36 M. Sánchez-Sánchez, N. Getachew, K. Díaz, M. Díaz-García, Y. Chebude and I. Díaz, *Green Chem.*, 2015, **17**, 1500-1509.

37 T. Rosinel and J. Rodriguez-Carvajal, *Proceedings of the Seventh European Powder Diffraction Conference (EPDIC 7)*, 2000, 118-123.

38 C. F. Macrae, P. R. Edgington, E. P. P. McCabe, G. P. Shields, R. Taylor, M. Towler and J. v. d. Streek, *J. Appl. Cryst.*, 2006, **39**, 453-457.

39 C. F. Macrae, I. J. Bruno, J. A. Chisholm, P. R. Edgington, E. P. P. McCabe, L. Rodriguez-Monge, R. Taylor, J. v. d. Streek and P. A. Wood, *J. Appl. Cryst.*, 2008, **41**, 466-470.

40 D. Zacher, J. Liu, K. Huber and R. A. Fischer, *Chem Commun.*, 2009, 1031-1033.

41 S. P. Diring, S. Furukawa, Y. Takashima, T. Tsuruoka and S. Kitagawa, *Chem. Mater.*, 2010, **22**, 4531-4538.

42 T. Borjigin, F. Sun, J. Zhang, K. Cai, H. Ren and G. Zhu, *Chem Commun.*, 2012, **48**, 7613-7615.

43 J. Jagiello and M. Thommes, *Carbon*, 2004, **42**, 1227-1232.

44 P. B. Balbuenat and K. E. Gubbins, *Langmuir*, 1993, **9**, 1801-1814.

Supplementary Information for

Particle size effects in the kinetic trapping of a structurally-locked form of a flexible metal-organic framework

Oliver M. Linder-Patton[a], Witold M. Bloch[a,b], Campbell J. Coghlan[a], Kenji Sumida[a], Susumu Kitagawa[c], Shuhei Furukawa[c], Christian J. Doonan[a] and Christopher J. Sumby[a]

[a.] *Department of Chemistry and Centre for Advanced Nanomaterials, School of Physical Sciences, The University of Adelaide, Adelaide, Australia. CJS: Fax: +61 8 8313 4358; Tel: +61 8 8313 7406; E-mail: christopher.sumby@adelaide.edu.au*

[b.] *Present address: Department of Chemistry, Georg-August-University Göttingen, Göttingen, Germany.*

[c.] *Institute for Integrated Cell-Material Sciences (WPI-iCeMS), Kyoto University, Kyoto, Japan.*

Structure determinations of solvent-exchanged forms of [Cu(bcppm)(H_2O)]

Full spheres of diffraction data were measured at *ca*. 150 K using CCD area-detector instrumentation on single crystals mounted on nylon loops in Paratone-N. All data were measured using monochromatic Mo-*K*α radiation, λ = 0.71073 Å. N_{tot} reflections were merged to N unique (R_{int} quoted) after multiscan absorption correction (proprietary software) and used in the full matrix least squares refinements on F^2, N_o with $F > 4\sigma(F)$ being considered 'observed'. In general, anisotropic displacement parameter forms were refined for the non-hydrogen atoms; hydrogen atoms were treated with a riding model [weights: $(\sigma^2(F_o)^2 + (aP)^2 + (bP))^{-1}$; $P = (F_o^2 + 2F_c^2)/3$]. Neutral atom complex scattering factors were used; computation used the *SHELXL97* program.[1] Pertinent results are given below, in the captions to Figures S1 and S2, and in Tables S1 and S2. CIF data (excluding structure factor amplitudes) have been deposited with the Cambridge Crystallographic Data Centre, CCDC reference numbers 1451302 [Cu(**bcppm**)(H_2O)]·acetone and 1451303 [Cu(**bcppm**)(H_2O)]·water**.** [Cu(**bcppm**)(H_2O)]·S (CCDC # 930403), [Cu(**bcppm**)(H_2O)]·ethanol (CCDC # 930405) and [Cu(**bcppm**)(H_2O)]-heated (CCDC # 930404) have been reported previously.[2]

Variata. In the crystal structure of [Cu(**bcppm**)(H_2O)]·$x$$H_2O$ 3½ well-ordered H_2O solvate molecules were located in the voids of the structure, however the relevant hydrogen atoms could not be located in the difference map.

Table S1. X-ray experimental data for solvent-exchanged forms of [Cu(**bcppm**)H_2O].

Compound	**[Cu(bcppm)H_2O]·acetone**	**[Cu(bcppm)H_2O]·water**
Empirical formula	$C_{30}H_{34}CuN_4O_8$	$C_{21}H_{30}CuN_4O_{12}$
Formula weight	642.15	594.032
Crystal system	orthorhombic	orthorhombic
Space group	*Pnma*	*Pnma*
a (Å)	10.2536(2)	9.4000(2)
b (Å)	19.8774(4)	19.5102(3)
c (Å)	14.8763(7)	14.7022(2)
Volume ($Å^3$)	3032.01(17)	2696.32(8)
Z	4	4
Density (calc.) (Mg/m^3)	1.407	1.429
Absorption coefficient (mm^{-1})	0.776	0.875
F(000)	1340	1180
Crystal size (mm^3)	0.19×0.15×10.12	0.18×0.29×0.46
θ range for data collection (º)	2.62 to 29.07	2.57 to 29.13
Reflections collected	14195	15996
Observed reflections [R(int)]	3623 [0.0420]	3341 [0.0314]
Goodness-of-fit on F_2	1.052	1.110
R_1 [I>2σ(I)]	0.0454	0.0354
wR_2 (all data)	0.1320	0.0996
Largest diff. peak and hole ($e.Å^{-3}$)	0.758 and -0.444	0.532 & -0.330

Structure descriptions of solvent-exchanged forms of [Cu(bcppm)(H_2O)]

The crystal structure of [Cu(**bcppm**)(H_2O)]·S has been previously reported,[2] but as it is the parent structure to the solvent-exchanged forms presented in this paper, it will be briefly described here. [Cu(**bcppm**)(H_2O)]·S crystallises in the orthorhombic space group *Pmna*, with half a molecule of the ligand **bcppm**, half a copper(II) atom, and half a water solvate molecule in the asymmetric unit. The copper(II) centre has a square pyramidal geometry and is coordinated by one chelating di-pyrazolylmethane unit, two monodentate carboxylate donors from two seperate molecules of **bcppm**, and a single water ligand. This gives rise to a charged balanced 2D MOF with a puckered 4-connected net (Figure S1) composed of chelating dipyrazolyl moieties that bridge to adjacent copper atoms *via* the monodentate carboxylate donors. An important feature of this family of materials is the eclipse of the 2-D layers which stack along the *a*-axis in an anti-parallel fashion. This gives rise to regular diamond shaped channels with dimensions of ~15×19 Å (depending on the solvate) propagating along the *a*-axis. While the structure has solvent accessible channels along the *a*-axis (Figure S1a), the *b* and *c*-axes [Cu(**bcppm**)(H_2O)]·S are essentially close-packed (Figure S1b and c).

A well-ordered water ligand is situated directly between the 2D layers, with a Cu-O bond length of 2.302 Å while the O-Cu distance to the above layer is 2.873 Å. The former length is well within the normal range for a Cu-O bond,[3] however, the latter is too distant for the geometry of the Cu(II) centre to be considered octahedral. The hydrogen atoms of this water ligand were successfully located in the difference map, and clearly to point towards the carbonyl oxygen atoms from an adjacent layer (Figure S1c). The O-H···O distance is 2.03 Å which is within the range of a moderate hydrogen bond.[4] Therefore, the eclipse of the 2D layers and formation of the 1D channels is driven by the puckering of the 2D nets and the strong interlayer hydrogen bonding between the hydrogen atoms of the water ligands in one layer and the carbonyl oxygen atoms from an adjacent layer. This water ligand is retained in all forms including the activated material.

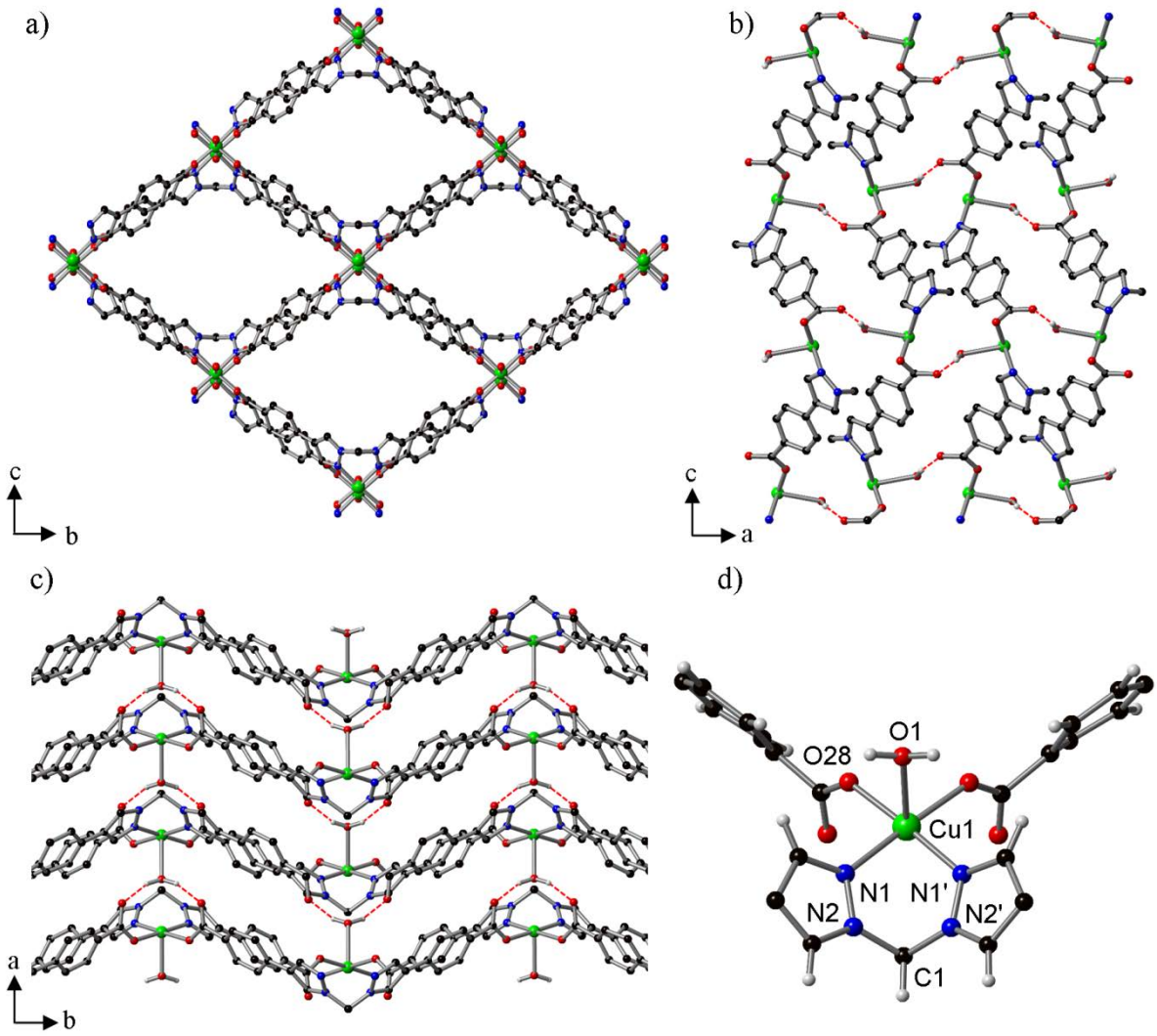

Figure S1. a) A view of the 1D channels of [Cu(**bcppm**)(H_2O)]·S along the *a* axis, b) a view along the *b* axis and c) a view along the *c* axis. Hydrogen atoms of **bcppm** are removed for clarity. (d) A view of the square pyramidal copper(II) centre of [Cu(**bcppm**)(H_2O)]·S. Hydrogen bonds are shown by the red dotted lines. Selected bond lengths [Å] and angles [°]: Cu1-N1 2.014, Cu1-O28 1.952, Cu1-O1 2.302, N2-C1-N2′ 107.50, N1-Cu1-N1′ 87.50.

The interlayer hydrogen bonding and the flexible chelating unit directly employed around the singular metal node led to an expectation of flexibility for the MOF structure. Solvent-exchanged forms of [Cu(**bcppm**)(H_2O)]·S were prepared by soaking batches of single crystals in acetone, water or ethanol before subjecting these to single crystal X-ray structure determinations. The structures are essentially isostructural, differing only in the nature of the included solvent (which was in some cases well

defined but in others subject to disorder), and particularly the extent of trellis-like breathing and layer-layer contraction. The crystallographic parameters of solvent-exchanged forms of [Cu(**bcppm**)H_2O] are given below in Table S2. [Cu(**bcppm**)(H_2O)]·acetone is essentially unchanged relative to the as-synthesised version with unit cell parameters given in Table S2 that reflect a small expansion of the *b* axis and a contraction of the *c* axis (see Figure S1a to understand these structural changes). There is a small expansion of the layer-layer separation too (increase in the *a* axis, see Figure S1c). [Cu(**bcppm**)(H_2O)]·water and [Cu(**bcppm**)(H_2O)]·ethanol are structurally similar with a shorter layer-layer separation than the as-synthesised form (*a* axis contraction) but a more significant trellis-like structural change (expansion of the *b* axis and a notable contraction of the *c* axis).

Table S2. Crystallographic parameters of solvent-exchanged forms of [Cu(**bcppm**)(H_2O)].

Form	**a (Å)**	**b (Å)**	**c (Å)**	**Volume (Å^3)**
[Cu(**bcppm**)(H_2O)]·S	9.9995	19.2590	15.4339	2955.13
[Cu(**bcppm**)(H_2O)]·acetone	10.2536	19.8774	14.8763	3032.01
Δ	*0.2541*	*0.6184*	*-0.5576*	*76.88*
[Cu(**bcppm**)(H_2O)]·water	9.4000	19.5102	14.7022	2696.32
Δ	*-0.5995*	*0.2512*	*-0.7317*	*-258.81*
[Cu(**bcppm**)(H_2O)]·ethanol	9.6611	20.3319	13.6276	2676.85
Δ	*-0.3384*	*1.0729*	*-1.8063*	*-278.28*
[Cu(**bcppm**)(H_2O)]-heated	8.8000	20.7340	13.1100	2392.04
Δ	*-1.1995*	*1.4750*	*-2.3239*	*-563.09*

[Cu(**bcppm**)(H_2O)]-heated, as previously reported,[2] undergoes the most significant change (Figure S2a vs. S2b) with a continuation of the structural modifications seen for the ethanol and water-exchanged samples but a dramatically shortened *a* axis cell length as a consequence of the water ligand now bridging between symmetry related copper(II) centres in adjacent layers (Cu1a-O1 = 2.265 Å, O1-Cu1 = 2.397 Å). This occurs with a change in the coordination environment of the copper(II)

centre from five coordinate to a Jahn-Teller distorted octahedral six coordinate (Figure S2c and S2d). The 3D structure that forms due to the coordination changes is also reinforced by noticeably shorter hydrogen bonding between the bridging water ligand and a carboxylate in the adjacent layer. The hydrogen bonds in [Cu(**bcppm**)(H_2O)]-heated are shortened by 0.3 Å relative to [Cu(**bcppm**)(H_2O)]·S giving a O-H···O distance of 1.73 Å.

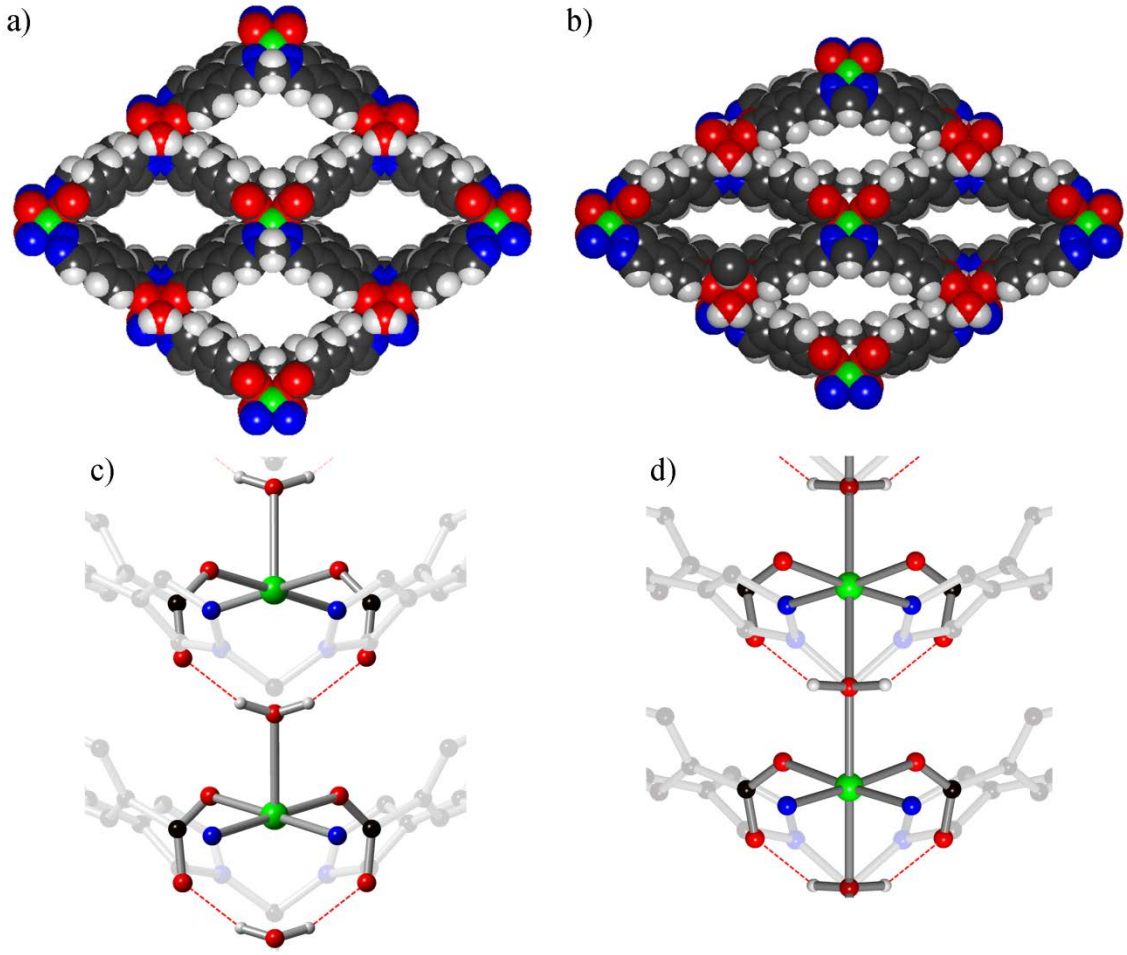

Figure S2. Space filling representations of a) [Cu(**bcppm**)(H_2O)]·S and b) [Cu(**bcppm**)(H_2O)]-heated viewed along the *a*-axis. The coordination environment of the copper(II) centre of c) [Cu(**bcppm**)(H_2O)]·S and d) [Cu(**bcppm**)(H_2O)]-heated. Red dotted lines denote hydrogen bonds.

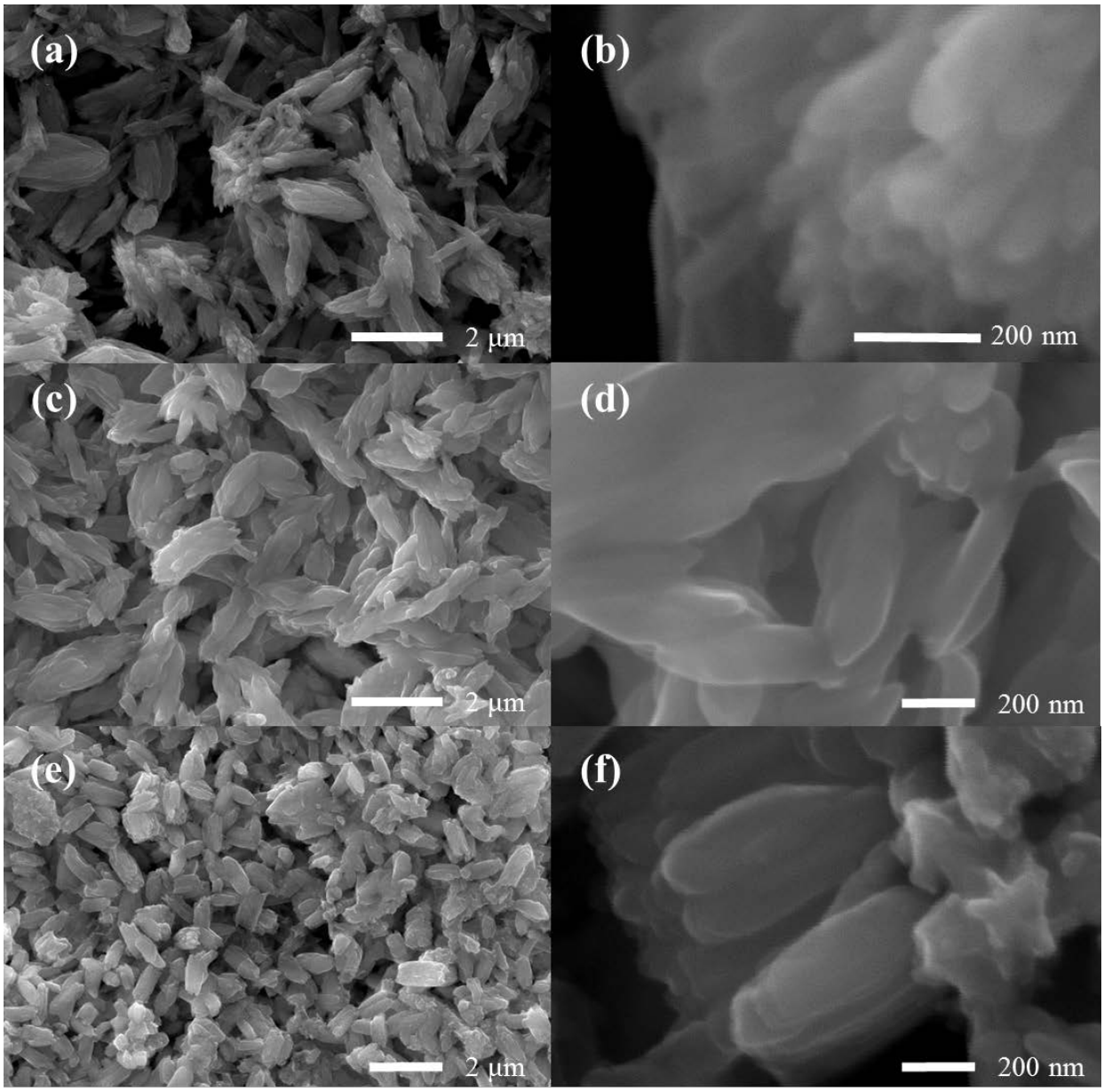

Figure S3. Additional SEM images of [Cu(**bcppm**)H_2O]·S synthesised at room temperature (a) & (b) with 0.1 M NaOH at 0.5 hrs, (c) & (d) 16 hrs, and (e) & (f) with Na_2**bcppm** at 16 hrs.

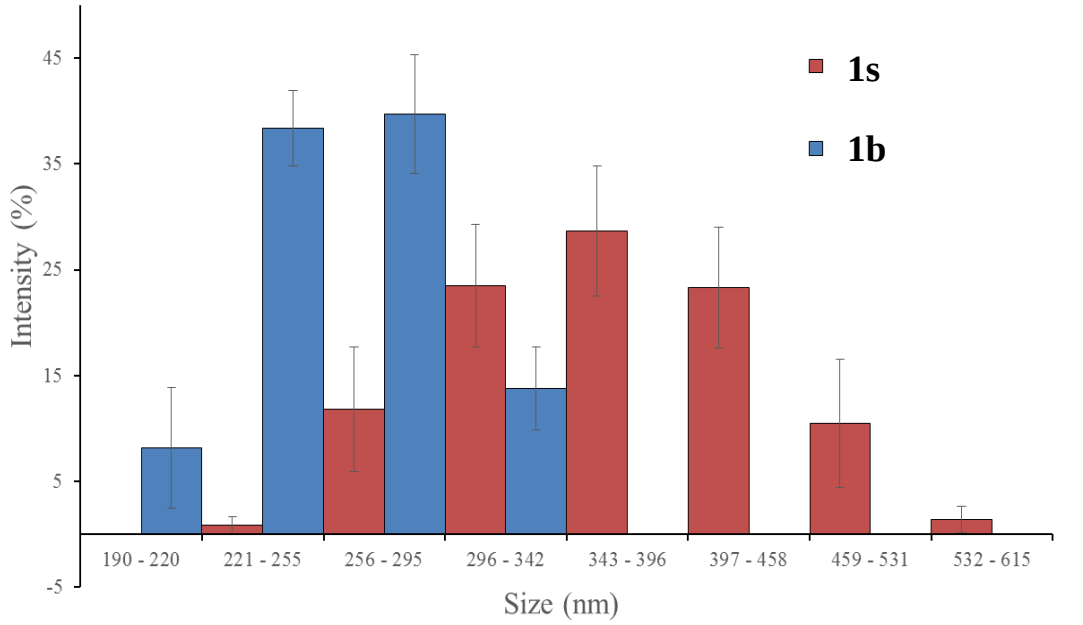

Figure S4. Average intensity from DLS experiments on samples of [Cu(**bcppm**)H_2O]·S synthesised at room temperature from 0.1 M NaOH (**1b**) and Na_2**bcppm** (**1s**) conditions.

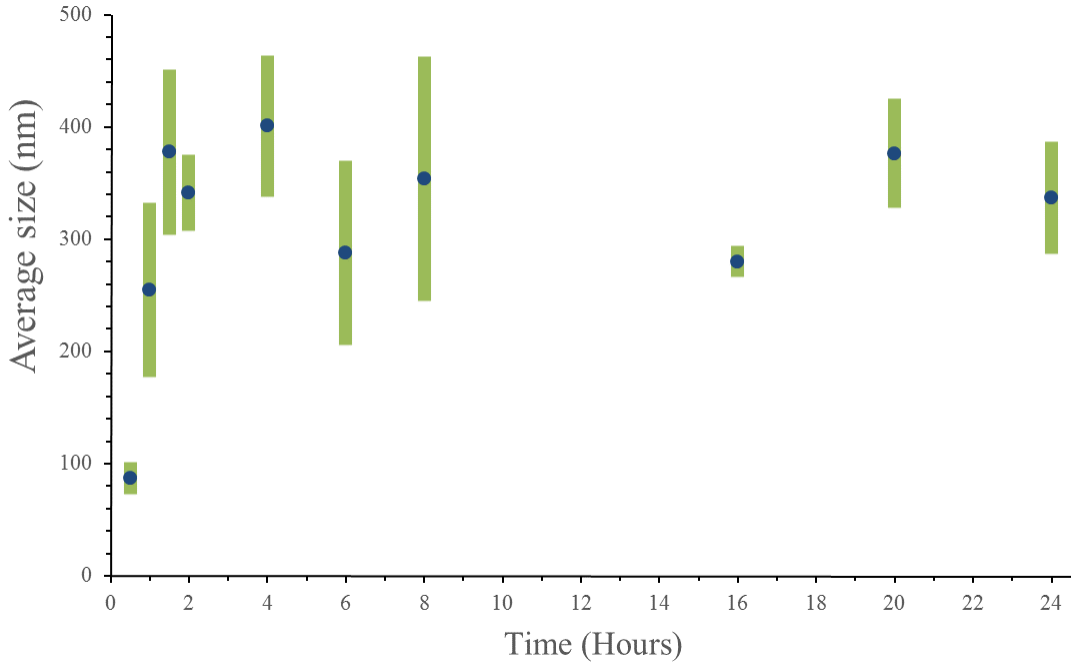

Figure S5. Average particle sizes determined from DLS experiments, demonstrating the growth of **1b**·S over 24 hours.

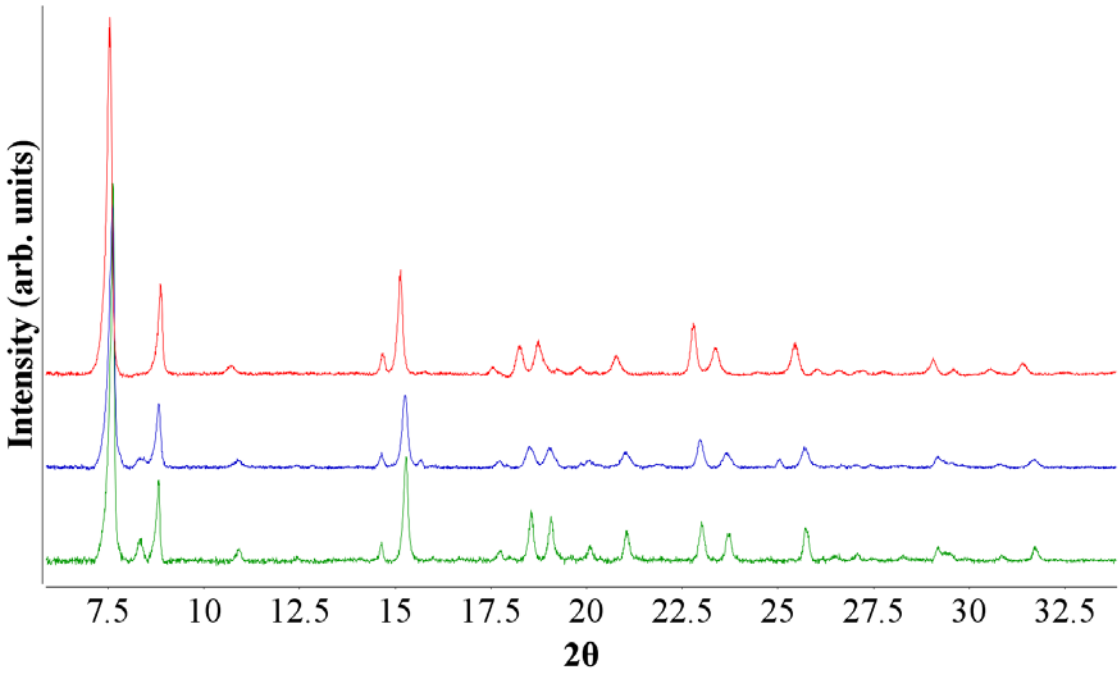

Figure S6. PXRD patterns of [Cu(**bcppm**)H_2O]·S solvothermally synthesised (green) (**1**·S), synthesised at room temperature with 0.1 M NaOH, 16 hrs, (blue) (**1b**·S) and with Na_2**bcppm** at room temperature, 16 hrs, (red) (**1s**·S). In the PXRD patterns presented the peaks at *ca.* 2θ = 7.5° and 2θ = 8.5° correspond to 011 and 020 planes respectively which reflect the breathing of the MOF. In the samples of **1**·S (green) and **1b**·S (blue) the peak at *ca.* 2θ = 8.0° corresponds to a small amount of the dried sample which forms as the material is packed into the capillaries.

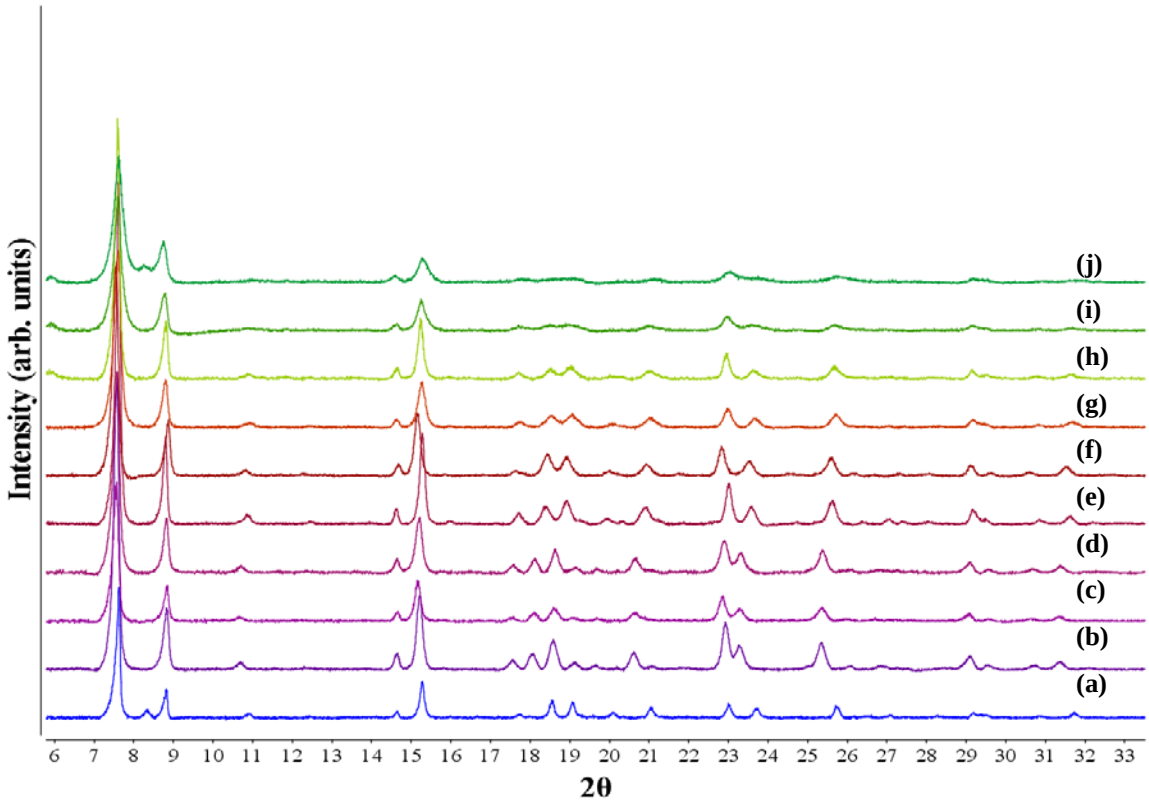

Figure S7. PXRD patterns of **1b**·S with varied reactant concentration and ligand-to-base (NaOH) ratio at 0.5 hrs, (a) normal solvothermal conditions **1**·S, (b) 36 mM ligand, 2:1, (c) 18 mM ligand, 2:1, (d) 12 mM ligand, 2:1, (e) 36 mM ligand, 1:1, (f) 18 mM ligand, 1:1, (g) 12 mM ligand, 1:1, (h) 36 mM ligand, 1:2, (i) 18 mM ligand, 1:2, (j) 12 mM ligand, 1:2. In the PXRD plots the peaks at *ca.* 2θ = 7.5° and 2θ = 8.5° correspond to 011 and 020 planes respectively which reflect the breathing of the MOF. In certain samples the peak at *ca.* 2θ = 8.0° corresponds to a small amount of the dried sample which forms as the material is packed into the capillaries.

General room temperature synthesis of [Cu(bcppm)H_2O]•S (S=solvate) with NaOH, 0.5 hrs (1b·S).

In a 20 ml screw cap vial, $Cu(NO_3)_2 \cdot 2½H_2O$ (36.0 mg, 0.16 mmol) and H_2**bcppm** (41.5 mg, 0.11 mmol) were dissolved in a mixture of DMF (2 ml) and ethanol (0.5 ml). Sodium hydroxide 0.1 M (0.5 ml) was injected into the stirring copper solution. The resultant solution was stirred for 0.5 h at room temperature. The product was washed with DMF (×2) and methanol (×5) resulting in a light blue microcrystalline material (8.0 mg, 16%).

Table S3. Varied reactant concentration and ligand-to-base ratio following the general experimental specified for the 0.5 hr room temperature reaction with 0.1 M NaOH.

$Cu(NO_3)_2 \cdot 2.5H_2O$		**H_2bcppm**			**DMF**	**EtOH**	**NaOH**		**Yield**	**Reaction time (min)**
(mg, mmol)		**(mM, mg, mmol)**			**(ml)**	**(ml)**	**(ml, molL^{-1})**		**(mg)**	
36.0	0.16	36	41.5	0.11	2	0.5	0.5	0.1	6	30
36.0	0.16	18	41.5	0.11	4	1	1	0.05	6	30
36.0	0.16	12	41.5	0.11	6	1.5	1.5	0.033	6	30
36.0	0.16	36	41.5	0.11	2	0.5	0.5	0.2	7	30
36.0	0.16	18	41.5	0.11	4	1	1	0.1	7	30
36.0	0.16	12	41.5	0.11	6	1.5	1.5	0.066	7	30
36.0	0.16	36	41.5	0.11	2	0.5	0.5	0.4	8	30
36.0	0.16	18	41.5	0.11	4	1	1	0.2	9	30
36.0	0.16	12	41.5	0.11	6	1.5	1.5	0.133	9	30

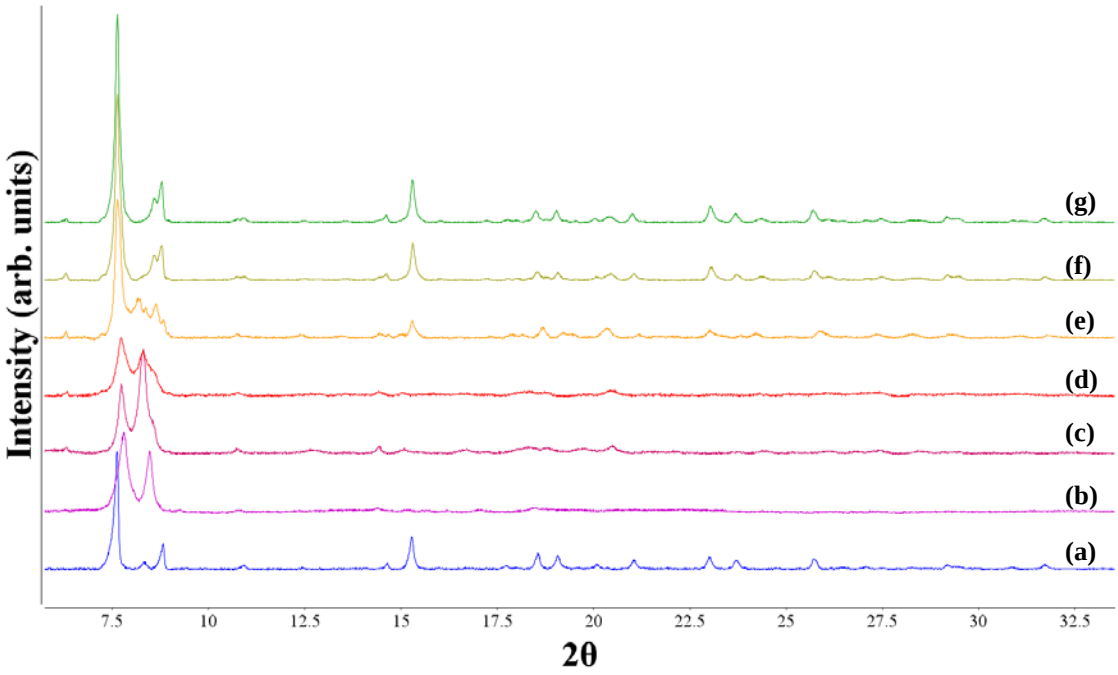

Figure S8. PXRD patterns of **1** (a) as-synthesised (methanol washed), (b) activated from acetone, resolvated in methanol for (c) 1 day, (d) 2 days, (e) 5 days, (f) 7 days and (g) 9 days. In the PXRD patterns the peaks at *ca.* 2θ = 7.5° and 2θ = 8.5° correspond to 011 and 020 planes respectively which reflect the breathing of the MOF. In the sample of **1**·S (blue) the peak at *ca.* 2θ = 8.0° corresponds to a small amount of the dried sample which forms as the material is packed into the capillaries.

(a)

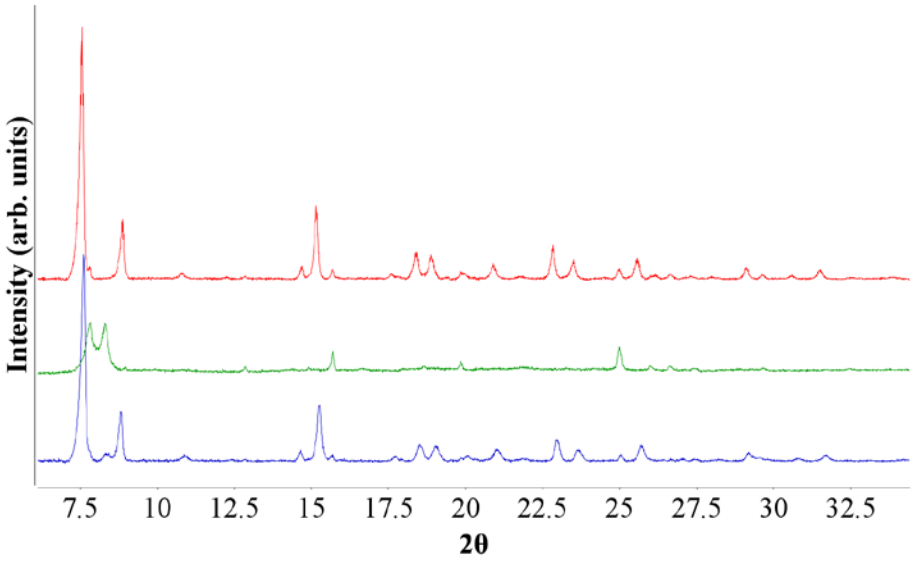

(b)

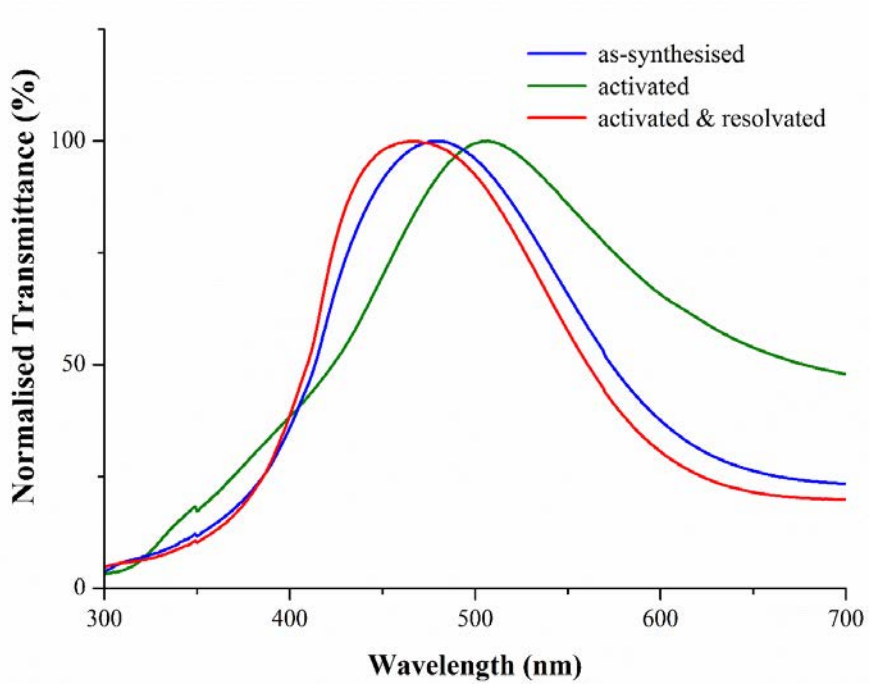

Figure S9. (a) PXRD and (b) solid state UV/vis transmittance spectra of **1b**·S as-synthesised (blue), activated (green) and activated and resolvated in methanol overnight (red). In the PXRD plots the peaks at *ca.* 2θ = 7.5° and 2θ = 8.5° correspond to 011 and 020 planes respectively which reflect the breathing of the MOF. In the sample of **1b**·S (blue) the peak at *ca.* 2θ = 8.0° corresponds to a small amount of the dried sample which forms as the material is packed into the capillaries.

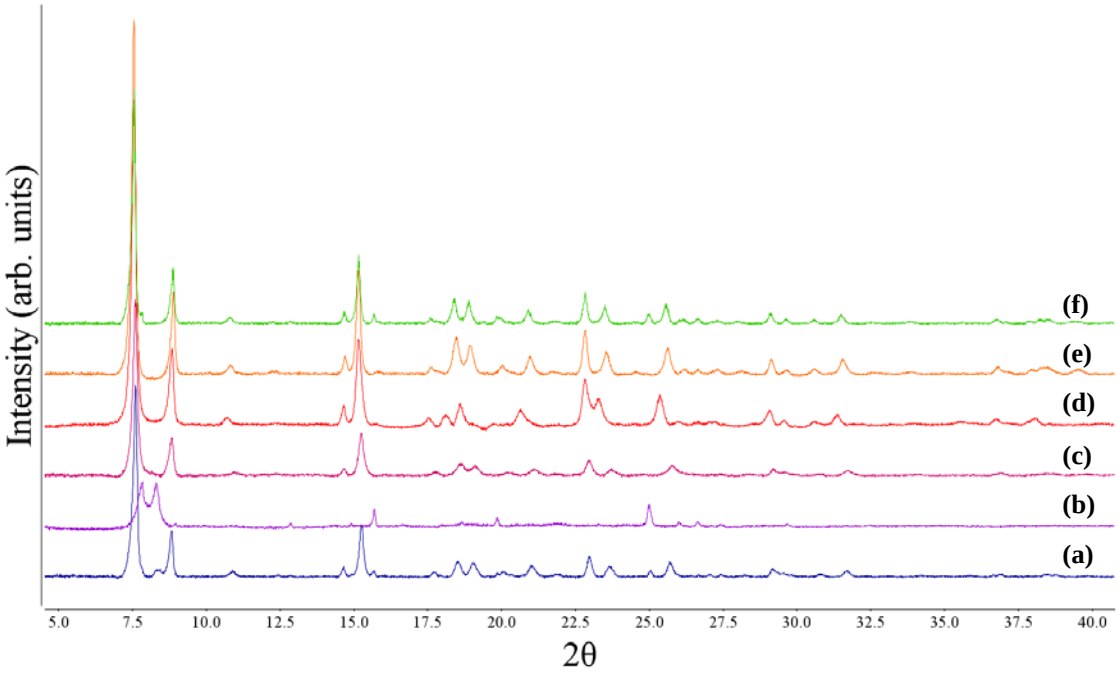

Figure S10. PXRD of (a) **1b**·S (at 16 h), (b) activated, activated and resolvated in methanol for (c) 1.5 h, (d) 3 h, (e) 4.5 h and (f) 16 h. In the PXRD plots the peaks at *ca.* 2θ = 7.5° and 2θ = 8.5° correspond to 011 and 020 planes respectively which reflect the breathing of the MOF. In the sample of **1b**·S (blue) the peak at *ca.* 2θ = 8.0° corresponds to a small amount of the dried sample which forms as the material is packed into the capillaries.

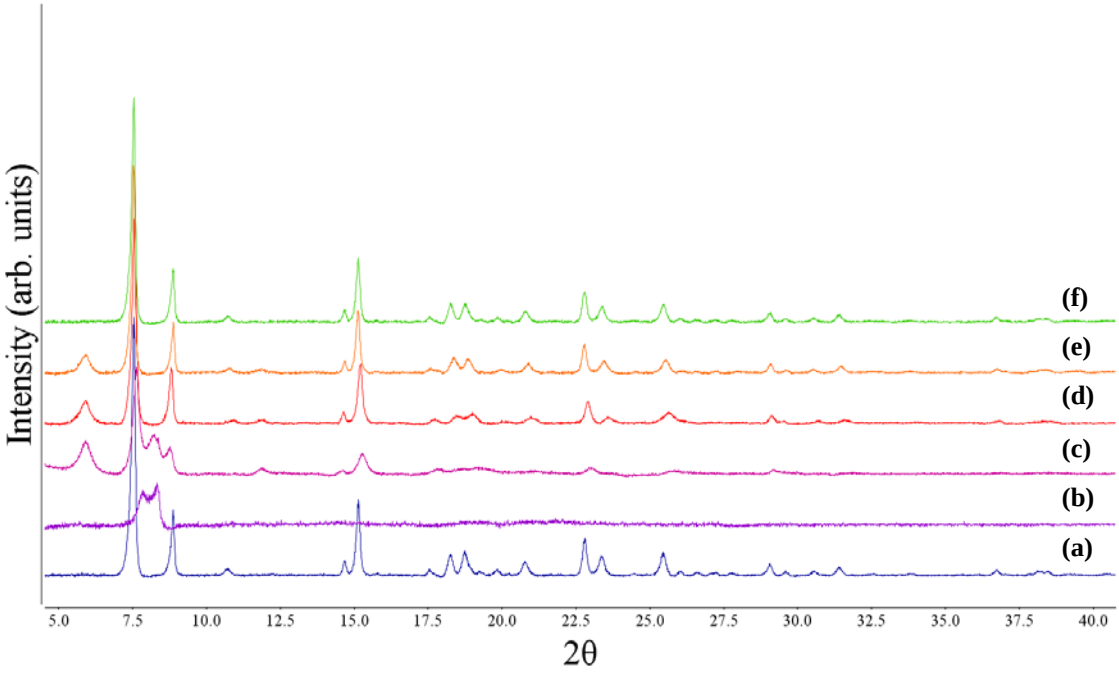

Figure S11. PXRD of (a) **1s**·S (at 16 h), (b) activated, activated and resolvated in methanol for (c) 1.5 h, (d) 3 h, (e) 4.5 h and (f) 16 h. In the PXRD plots the peaks at *ca.* 2θ = 7.5° and 2θ = 8.5° correspond to 011 and 020 planes respectively which reflect the breathing of the MOF.

(a)

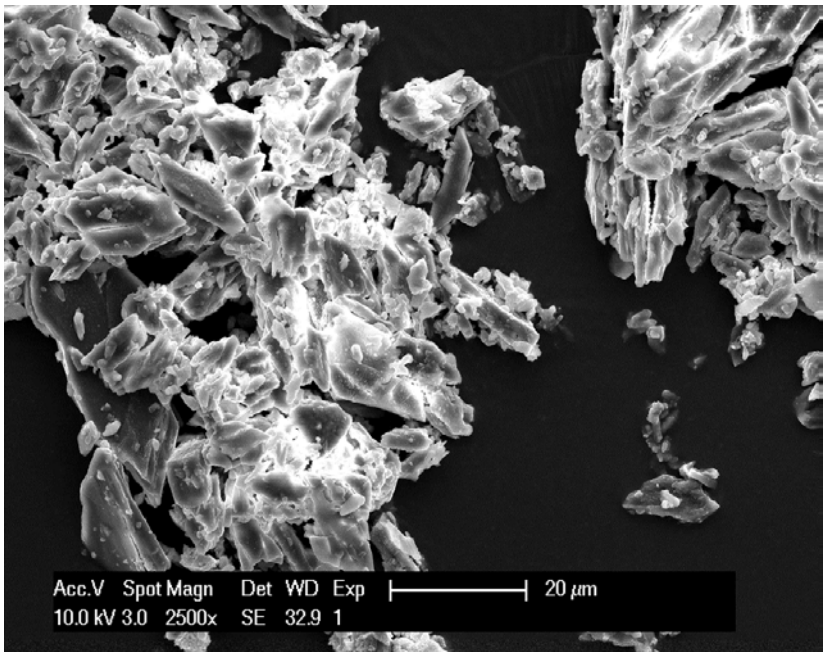

(b)

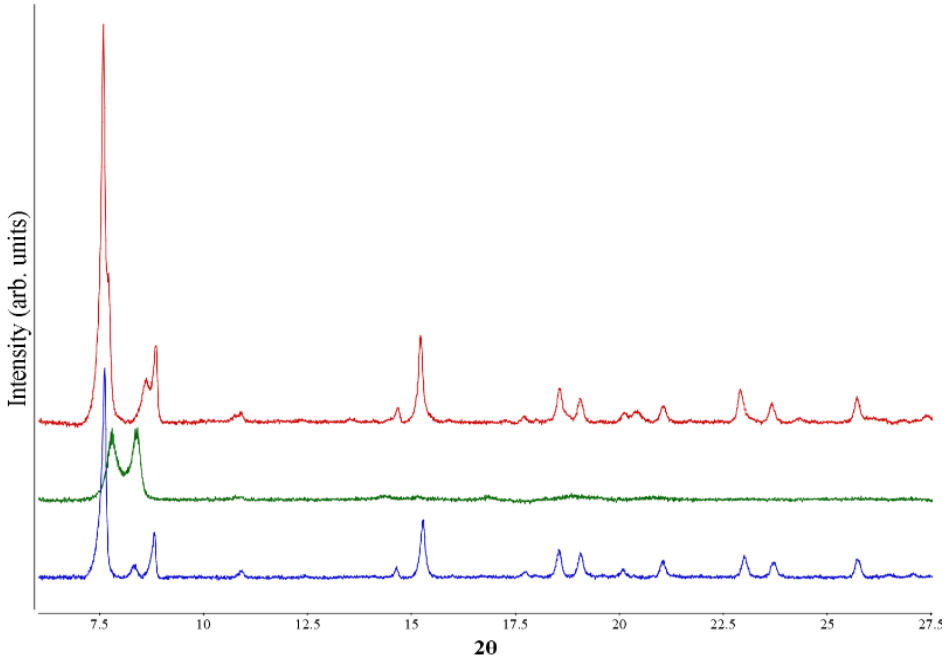

Figure S12. (a) SEM image and (b) PXRD patterns of **1**·S solvothermally synthesised and manually crushed (blue), activated (green) and, activated and resolvated overnight (red). In the PXRD plots the peaks at *ca.* 2θ = 7.5° and 2θ = 8.5° correspond to 011 and 020 planes respectively which reflect the breathing of the MOF. In the sample of **1b**·S (blue) the peak at *ca.* 2θ = 8.0° corresponds to a small amount of the dried sample which forms as the material is packed into the capillaries.

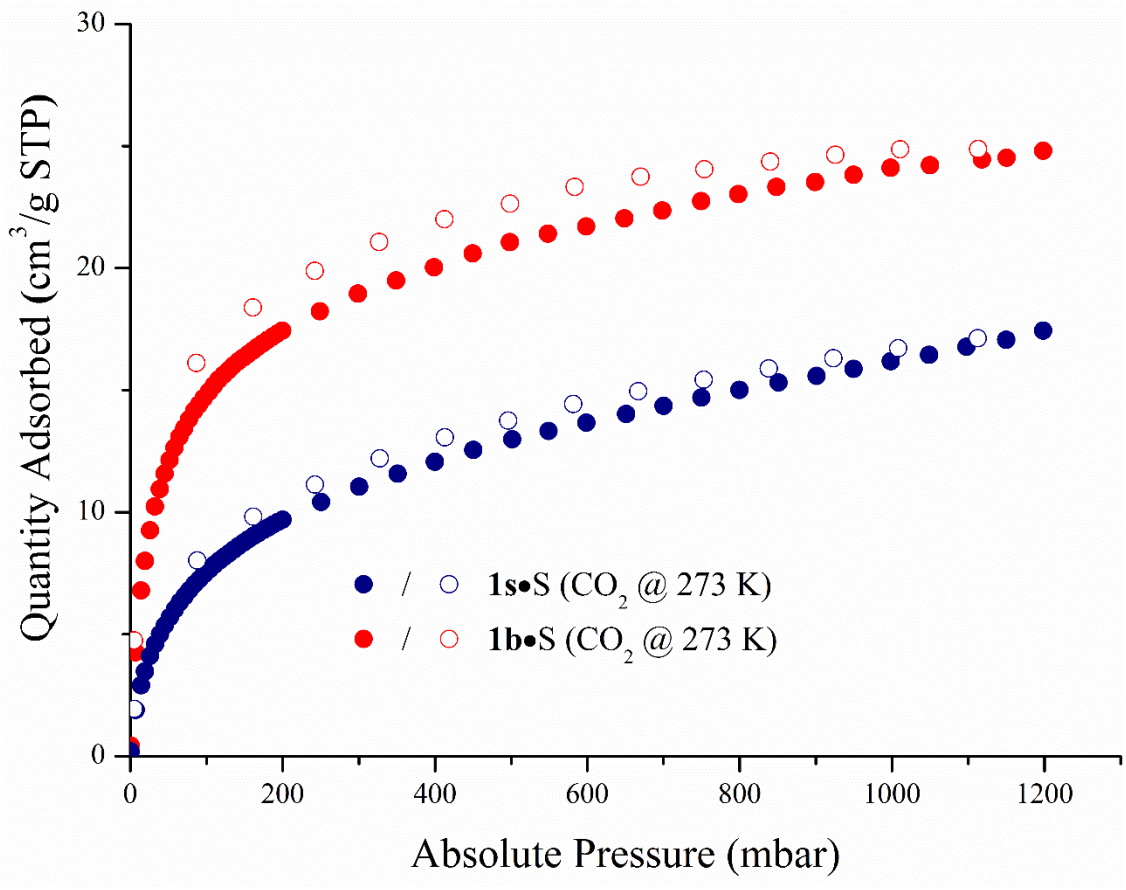

Figure S13. 273 K CO_2 isotherms of **1b**·S (blue) and **1s**·S (red). Adsorption = filled circles; desorption = open circles.

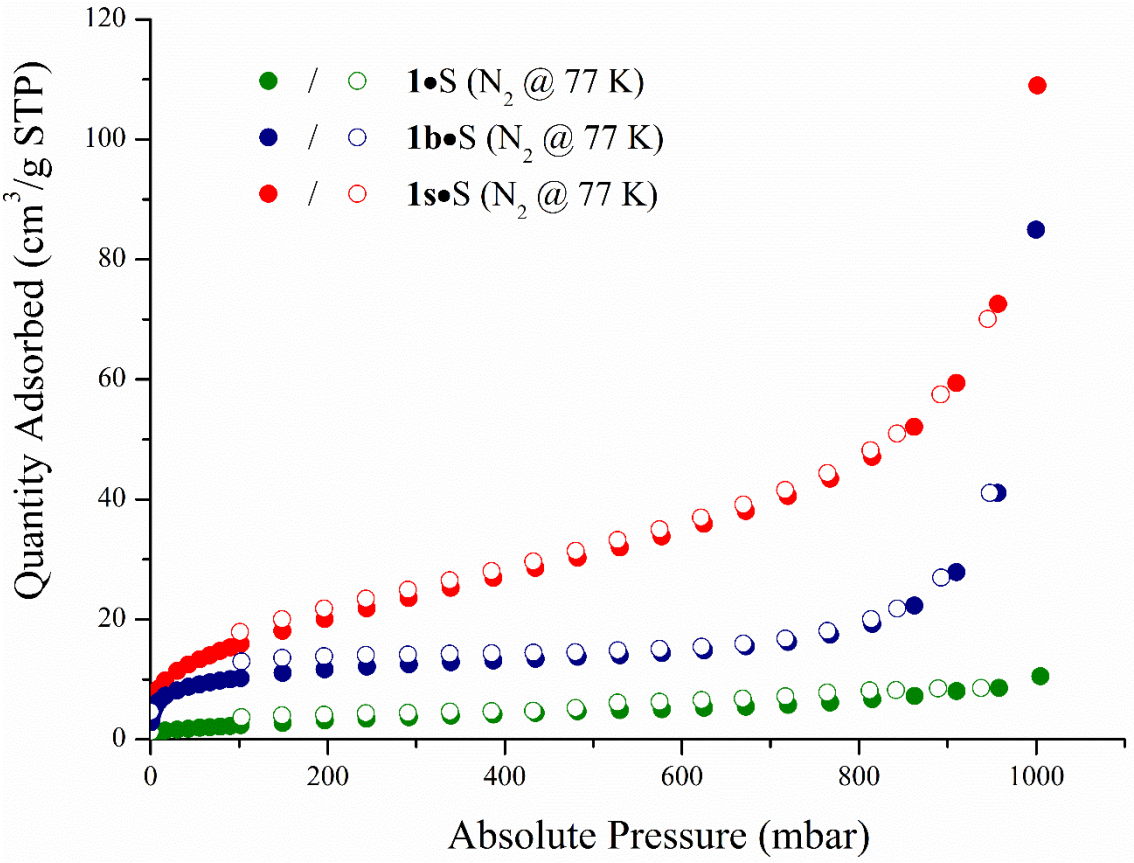

Figure S14. 77 K N_2 isotherms of **1**·S (green), **1b**·S (blue) and **1s**·S (red). Adsorption = filled circles; desorption = open circles.

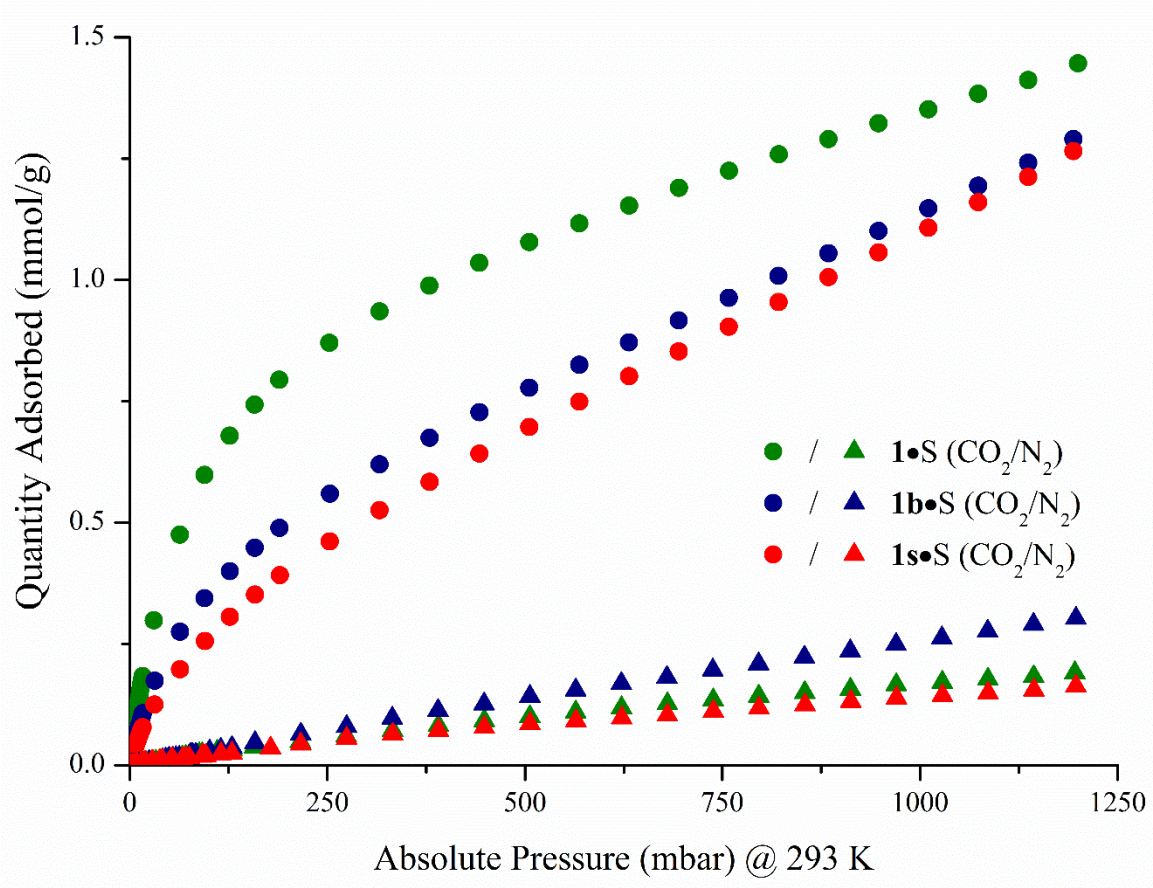

Figure S15. 293 K CO_2 and N_2 isotherms of **1**·S (green), **1b**·S (blue) and **1s**·S (red). Adsorption = filled circles; desorption = open circles.

Table S4. IAST selectivity data for **1**·S, **1b**·S and **1s**·S.

Sample	Crystal size (nm)	Selectivity (CO_2/N_2)[a]
1·S	50000	100
1b·S	402	40
1s·S	280	65

a. 15/85 wt% mixture at 293 K and 1 atm

References

1. G. M. Sheldrick, Univ. Gottingen, Gottingen, Germany, 2014; *Acta Crystallogr*. 2008, **A64**, 112; *Acta Crystallogr*. 2015, **C71**, 3.
2. W. M. Bloch, R. Babarao, M. R. Hill, C. J. Doonan and C. J. Sumby, *J. Am. Chem. Soc.*, 2013, **135**, 10441.
3. I. M. Procter, B. J. Hathaway and P. Nicholls, *J. Chem. Soc., A: Inorg. Phys. Theor.*, 1968, 1678.
4. G. R. Desiraju and T. Steiner, *The Weak Hydrogen bond: In Structural Chemistry and Biology*, Oxford University Press, United States, New York, 2001.